Graded PVD Mo-Si interlayer between Si coating and Mo-Si-B alloys: investigation of oxidation behaviour

Ronja Anton [a,*], Steffen Hüning [b], Nadine Laska [a], Matthias Weber [c], Steven Schellert [c], Bronislava Gorr [d], Hans-Jürgen Christ [c], Uwe Schulz [a],

[a] German Aerospace Center (DLR), Institute of Materials Research, Cologne, 51147, Germany

[b] Technical University (TU) Dortmund, now LIMO GmbH, Dortmund, 44319, Germany

[c] Institute for Materials Engineering, University of Siegen, Siegen, 57076, Germany

[d] Institute for Project Defaults, Karlsruhe Institute of Technology (KIT), 76131 Karlsruhe, Germany

*Corresponding author. E-mail address: ronja.anton@dlr.de (R. Anton).

Abstract

The insufficient oxidation resistance of Mo-Si-B alloys at high temperatures inevitably requires a protective coating. A dual layer system combining a graded Mo-Si interlayer with a Si oxidation protective top layer has been applied by magnetron sputtering on a Mo-9Si-8B alloy. The interlayer architecture was designed to maximize the adhesion between top layer and substrate by creating thermodynamic compatibility between alloy and Si. Isothermal oxidation tests at 800 and 1200 °C in air up to 300 h were performed focusing on chemical reactions between top layer, interlayer and substrate as well as the evolution of the thermally grown SiO_2.

Keywords: physical vapour deposition, silicon dioxide, oxidation protection, silicon, Mo-silicide

1. Introduction

Mo-Si-B alloys are extremely attractive for use in aircraft turbines due to their mechanical properties including excellent creep resistance and strength retention at high temperatures [1]. These properties can primarily be attributed to alloys from the Mo_{ss} - Mo_3Si - Mo_5SiB_2 phase region [2-4]. The purely intermetallic Mo_3Si and Mo_5SiB_2 phases exhibit better high-temperature resistance, but are significantly more brittle than the Mo_{ss}. This is due to the complex crystal structure and the strong bonding forces between the atoms of the intermetallic phases [5-7]. In addition, these properties are also responsible for the excellent creep resistance of the intermetallic phases, especially the T2 phase Mo_5SiB_2, at high temperatures. Good creep resistance is particularly important for turbine blades under high thermal and mechanical loading [1, 8, 9]. Equally important for technical applications is the ductility of the material, which is primarily achieved by the Mo_{ss} phase [10, 11]. The oxidation behaviour of Mo-Si-B alloys can generally be divided into two oxidation stages. In the intermediate temperature range below 1000 °C, a reaction-controlled behaviour is present due to MoO_3 evaporation. As a result, substantial mass loss and catastrophic oxidation as well as so-called pest oxidation can occur [5, 12-14]. At higher temperatures above 1000 °C, a diffusion-controlled steady state is established due to the formation of a borosilicate layer [15, 16]. Accordingly, the mass loss is directly dependent on how fast the covering borosilicate layer spreads. In the temperature range between 1000 and 1700 °C, the $MoSi_2$ phase has a permanent oxidation resistance, which is due to the formation of a parabolically growing SiO_2 top layer [12]. By alloying theses alloys with titanium, the oxidation and the creep behaviour can be somewhat improved [17-22]. Overall,

the necessity of a protective coating becomes inevitable. A proper performance of the coating can be ensured by a thermochemical compatibility between the coating and the alloy as well as by its coefficient of thermal expansion (CTE). The CTE should be close to that of the Mo-Si-B-alloys. Oxidation protective coatings for Mo-Si-B-based alloys are largely synthesised by means of a chemical vapour deposition (CVD) process called pack cementation. Several studies using Al- and Si-based coatings have been published [4, 23, 24]. Co-pack cementation of Si, Si and B, or Si and Al is used to produce the CVD coatings. The coatings have to be heat treated after deposition. While testing, the coatings show either an oxidation protective layer based on borosilicate, SiO_2 or Al_2O_3 [23, 25-27]. Other processes showed potential for the successful deposition of Si-containing oxidation protection layers. For example, plasma cladding (PTA) was used to produce layers of Mo_3Si with dispersed Mo_5Si_3 particles. With the addition of small amounts of boron and the resulting formation of a borosilicate glass layer, oxidation resistance of the layers was demonstrated at 1300 °C [28]. Nomura et al. applied Mo-Si-B coatings consisting of the phases Mo_5Si_3, Mo_3Si and Mo_5SiB_2 by low-pressure plasma spraying on a Mo-ZrC substrate. The formation of a passivating borosilicate glass layer could prevented oxidation at temperatures of 1400 °C [29]. Compared to CVD coatings, plasma sprayed coatings have increased porosity, which favours oxygen inwards diffusion. This leads directly to the degradation of the oxidation protection layer. Polymer-derived ceramic protective coatings were developed for Mo-based alloys by Smokovych et al. Here, mainly the oxidation behaviour of the coatings in the range of 800 °C was investigated [30, 31]. Furthermore, oxidation protection layers for Mo-Si-B alloys can be deposited by means of magnetron sputtering [2, 32, 33]. Lange et al. applied coatings of the compositions Mo-70Al, Mo-37Si-15B and Mo-46Si-24B with thicknesses of 5-10 µm on Mo-9Si-8B substrate and investigated their oxidative properties at 800, 1000 and 1300 °C in air atmosphere. Due to the relatively low coating thicknesses, the lifetime of the protective coatings was substantially limited by interdiffusion with the substrate alloy [2].

In our previous work [34], single layers of pure Si have been applied on Mo-9Si-8B substrates for the first time by magnetron sputtering. As a result of the surface-grown SiO_2 layer, the alloy could be protected from oxidation for up to 300 hours at 1200 °C. At intermediate temperatures of 800 °C, pest oxidation was successfully suppressed for a period of up to 100 hours. A thin interdiffusion zone of Mo_3Si developed. In this paper, thin film systems containing Mo-Si were applied on TZM and on the alloy Mo-9Si-8B by means of magnetron sputtering with the objective of preventing oxidative attacks on the base material. An additional interlayer between the substrate and the Si oxidation protection top layer is introduced, intended to provide thermodynamic equilibrium between the Mo-based alloys and Si. Furthermore, the CTE mismatch of the Mo-9Si-8B alloy and the Si top layer as well as the tensile stress this can create should be minimized and compensated through the interlayer. The interlayer is designed to develop the $MoSi_2$ phase before the coating of pure Si as oxidation protection follows. In case the Si coating fails, the $MoSi_2$ layer can also withstand the oxygen attack as emergency running feature because of its oxidation protection properties. The interlayer is Mo-Si graded starting at a composition close to Mo_5Si_3, $MoSi_2$ and ending with pure Si. The silicon top layer is distinguished by introducing a slightly porous morphology to possibly withstand against greater stresses as well as protecting against oxidation.

2. Material and methods

The fabrication of the Mo-9Si-8B alloy (in at.%) has been done at Karlsruher Institute of Technology (KIT) by arc melting (AM/0.5, Edmund Buehler GmbH). The respective purities of the used elements are 99.99 % (Mo), 99.8 % (Si), and 99 % (B). The production was complete in a water-cooled Cu crucible operating within an Ar atmosphere [34, 35]. Contaminations by oxygen of the substrate material was routinely

controlled by hot gas carrier extraction during arc melting. An oxygen content of 150 to 350 wt ppm is usually detected. For comparison, the powder metallurgy process reaches an oxygen content above 2000 wt ppm. [34, 36]. To ensure a homogenous elemental distribution the melting procedure was repeated multiple times. The produced Mo-9Si-8B alloy contained the phases Mo_{ss} (bcc), Mo_3Si (A15), and Mo_5SiB_2 (T2) [24]. Mo-9Si-8B substrates with dimensions of about 10 x 15 x 2 mm have been used in the as-cast state. Since the sample had to be electric discharge wire cut out of the arc melted bar the dimension can slightly change to increase sample size. Furthermore, a commercial titan–zirconium–molybdenum alloy (TZM) (Plansee AG, Reutte, Austria) with the nominal composition of Mo-0.5 Ti-0.08 Zr-0.01–0.04 C (in at.%) has been investigated mainly for the analytical work in the as-coated condition. For the production of the Mo-Si interlayer as well as the Si top layer, a batch-type magnetron sputtering facility (IMPAX, Systec SVS vacuum coatings, Karlstadt, Germany) had been chosen. The samples have been attached to a wire for the purpose to coat as much surface as possible. Before coating deposition, specimens were prepared by grinding until 900 grid and subsequently cleaned in ethanol and water. The cleaning of the specimen in the PVD chamber by Ar^+-ion etching also activates the specimen surface. For this purpose, a negative bias voltage of 500 V was applied to the substrates and Ar^+ ions were accelerated towards the substrate surface at an Ar flux of 300 sccm under a 100 KHz pulse frequency with a pulse duration of 1 µs. The whole process was done under a vacuum pressure of 6.3 10^{-3} mbar. Dense polycrystalline targets of Si and Mo were utilized. The application of the oxidation protection top layer was done exclusively by means of one Si-targets. The targets (Evochem Advanced Materials GmbH Offenbach, Germany) have a purity of 99.999 % (Si) and 99.95 % (Mo). The targets of IMPAX have an area of 200 cm^2 (20 × 10 cm^2). For the production of the Mo-Si interlayer, one sample holder was positioned between the Mo and Si targets in such a way that a minimal distance of 225.5 mm between rotary axis and the two targets were established. A two-fold rotation was applied so that every surface of the samples was coated homogeneously. While the Si-target was supplied with a constant power of approx. 1.2 kW, the Mo-target was gradually reduced by 0.2 kW each in a cycle of two hours with the aim to successively adjust a graded interlayer, starting at a power of 1.1°kW. The power was set in such a way that the layer composition was gradually varied from a Mo_5Si_3 phase to $MoSi_2$ and finally to a pure Si layer. The interlayer was manufactured by applying an additional substrate heating of approximately 500 °C. After switching off the Mo target power, the samples were positioned in front of the Si target, for the deposition of pure silicon top layer at a distance of 150 mm to increase the deposition rate. The application of the top layer was carried out over a period of about 7 hours at a constant substrate temperature of 150 °C. During the coating process, a constant bias voltage of 50 V for the interlayer and 100 V for the top layer was permanently applied to the substrates.

A crystallization treatment was applied for 1 hour at 900 °C in air because the Si top layer coating was X-ray amorphous after the deposition process. Since the morphology does not show any significant changes no investigation after crystallization is shown. A rapid heating up had been chosen during crystallization to achieve a rapid densification of the coating towards the surface by closing the intercolumnar gaps. Based on previous data obtained, 900 °C was chosen to ensure the crystallization of Si. The pest oxidation resistance of the coating had been tested at 800 °C while high temperature oxidation behaviour was carried out at 1200 °C. The coated Mo-9Si-8B specimens underwent immediately after crystallization isothermal oxidation testing for either 10, 100 or 300 hours at 1200 °C in lab air in a box furnace without cooling between the crystallization and oxidation. In addition, the uncoated alloy was oxidized as well but without crystallization. The mass change has been documented for every specimen. To analyse the sample further a new sample had to be used for every time frame. Samples that run for longer times have not been cooled in between, therefore a continuous isothermal oxidation has been applied. Since the samples are normed by

given mass per surface area a continuous mass change curve has been constructed. Coated and un-coated samples have been oxidized at 800°C for 100 hours, again without cooling the samples in between.

Using the scanning electron microscopy (SEM) (DSM Ultra 55, Carl Zeiss NTS, Wetzlar, Germany) equipped with an energy-dispersive X-ray spectroscopy (EDS) system (Aztec, Oxford Instruments, Abingdon, UK), the microstructural analyses could be performed for all coatings. EDS measurements have been realized at 15 kV. In order to analyse the phase formation, XRD (Bruker D8 Advance, Cu Kα radiation, EVA/Topas 4.2 software package, Bruker AXS, Karlsruhe, Germany) has been carried out. The production of a lamella using a focused ion beam (FIB) (Dual Beam FEI Helios, FEI Philips, The Netherlands) led to the analysis of the interdiffusion zone (IDZ) with a transmission electron microscopy (TEM) at University of Siegen. There, imaging, scanning transmission electron microscopy (STEM) EDS analyses and electron diffraction measurements applying selected area diffraction (SAD) (Talos F200 kV FEI, The Netherlands) had been conducted.

3. Results

3.1. Microstructure of the dual layer system after deposition

Fig. 1 a) shows the dual layer system in the initial state, further on described as as-coated, on the commercial Mo substrate material TZM. The coating has a thickness of about 20 µm in total. The microstructure of the deposited dual layer system in its initial state system consists of columns typical for PVD layers especially in the fracture surface (Fig. 1 a)) and the top view (Fig. 1 c)).

When looking at the interlayer, a rather dense and homogeneous structure can be seen in the area close to the interface to the base material. As the layer thickness increases, a columnar structure typical for PVD coatings continuously forms with a certain growth direction of the columns. The width of the individual columns increases in line with the height. In addition to the columnar growth, irregular larger spaces between the columns of divergent size less than 500 nm occur and become larger with thickness. The interstitial spaces disappear with the deposition of the pure Si on top of the interlayer structure and only show intercolumnar gaps less than a few nanometers (Fig. 1 a)). In contrast to the columns of the Mo-Si graded interlayer, those of the Si top layer have a continuous vertically oriented structure with column widths of approx. 2 - 2.8 µm. These are also clearly visible in the top view of the layer surface (Fig. 1 c)). Here, a flat but nevertheless cauliflower-like surface morphology is shown which is common for PVD coatings. Furthermore, the inter-columnar gaps can also be seen in the top view. The resulting structure continues for almost the entire surface. Only occasionally inhomogeneities occur in the form of relatively large and exaggerated columns as well as wide column gaps, both are most likely triggered by surface irregularities.

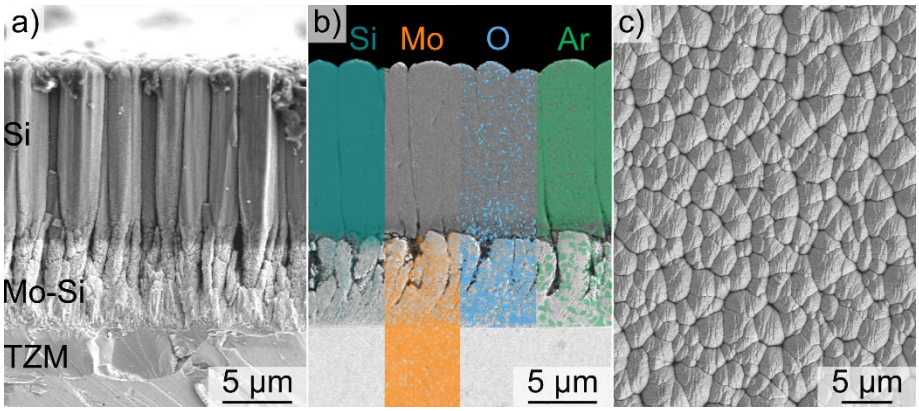

Fig. 1. Secondary electron micrograph (SEM) of dual layer system after deposition by magnetron sputtering; a), the fracture surface of the coating; b) polished cross section with EDS element distribution image in at.%; c) in top view, deposited on a TZM substrate.

Fig. 1 b) shows the EDS element distribution in at.% over the complete layer thickness. Fig. 2 supplements the results with an EDS line scan demonstrating the distribution of the involved elements graphically. Starting in the TZM alloy the interlayer is clearly marked by a rapid decrease in Mo and an instant increase in Si. This trend continues throughout the interlayer. Due to the curved growth of the interlayer columns the gradation of the interlayer is not perfectly displayable. The Mo content gives an idea of the Mo_5Si_3 to $MoSi_2$ ratio rather than the Si content. Furthermore, a not inconsiderable amount of up to 20 at.% oxygen was detected in the interlayer already in the as-coated state, but only in areas where the Mo content is dominant. When silicon takes over as the major constituent, the oxygen content decreases drastically. Within the Si top layer, the oxygen content goes to zero whereas the Ar content is detectable by about 3 – 4 at.%.

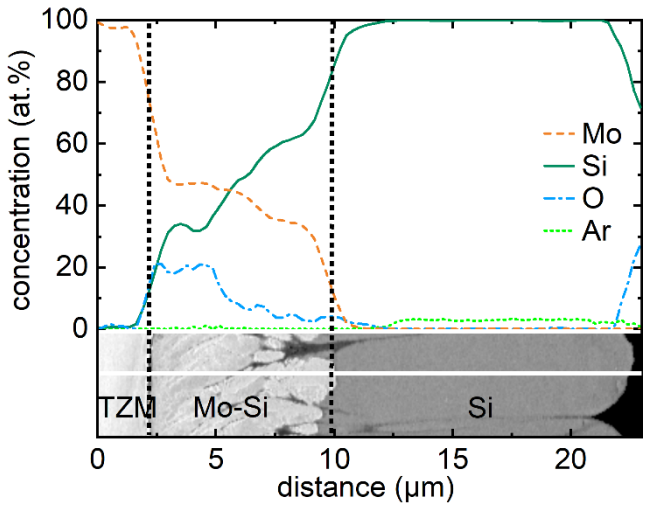

Fig. 2. SEM-EDS line scan in at.% of dual layer system in the as-coated state.

3.2. Oxidation behaviour of the dual layer after isothermal oxidation testing in air

Fig. 3 shows SEM images of cross-section of the dual layer system deposited on the substrate alloy Mo-9Si-8B, which were crystallization heat treated at 900 °C and immediately isothermally aged in laboratory air at 1200 °C for 10, 100 and 300 hours. Already after 10 hours (Fig. 3 a)) a distinct change of the Si top layer structure can be seen in comparison to the as-coated state (Fig. 1 b)). The columnar gaps are almost completely closed and a microporous structure becomes visible. Furthermore, a homogenous, dense and

fully covering SiO_2 thermally grown oxide (TGO) layer develops on the Si top layer. After 10 and 100 hours (Fig. 3 a) and b)), additional formation of SiO_2 is visible as bands that run vertically along the original column spaces and partially reach the interlayer, details follow in (Fig. 5 b), c)). Over time, the size of the pores in the Si top layer have visibly increased after 300 hours of exposure (Fig. 3 c)). These pores are partially interconnected and partially filled with preparation residues in the sectional plane. Using EDS analysis, up to approx. 1 at.% argon could be detected in the Si top layers.

A significant change in the layer structure is also visible in the interlayer area. The Mo-Si columns brightly displayed on the SEM images show a considerable reduction in width and homogeneity. With increasing exposure time, the structure, which was barred in the initial state, increasingly dissolves and molybdenum-containing isles have form, especially after 300 hours (Fig. 3 c)). The interface between interlayer and substrate is visible due to thin line of small SiO_2 precipitates. With increasing testing time, they agglomerate.

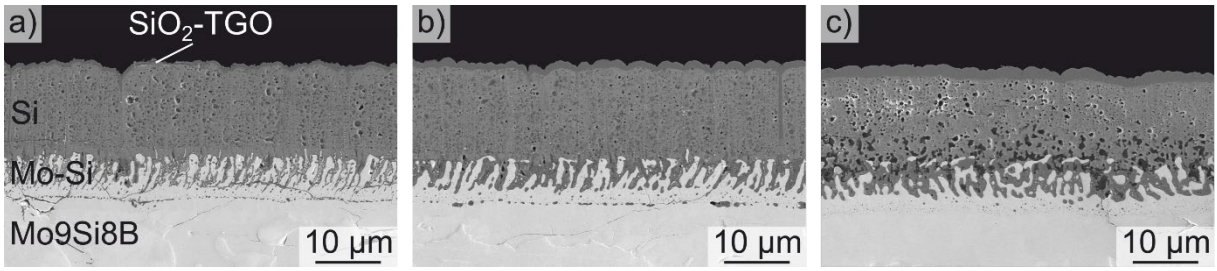

Fig. 3. Secondary electron SEM cross-sectional images of the dual layer system's evolution of the microstructure, deposited on Mo-9Si-8B, after 10 a), 100 b) and 300 hours c) istothermal exposure time at 1200 °C in laboratory air.

As a result of the oxidation tests, a homogeneously distributed and dense thermally grown oxide layer grows on all Si top layers. Fig. 4 shows the evolution of the TGO layer of the dual layer system on the Mo-9Si-8B alloy with increasing holding time. It can be seen that after only 10 hours (Fig. 4 a)) an about 0.75 µm thin but completely closed layer of SiO_2 forms on the Si top layer. After 300 hours of testing, local vertical segmentation cracks appear within the TGO layer (Fig. 4 c)). Below these cracks, no accelerated internal oxidation of the silicon could be detected, which suggests that these cracks only developed during the cooling phase and not during the high-temperature oxidation test. EDS point analysis within the TGO was able to determine a chemical composition of up to 65 at.% oxygen and about 35 at.% silicon, which correspond to the X-ray diffraction measurements (Fig. 6) and identifies the silicon dioxide as cristobalite.

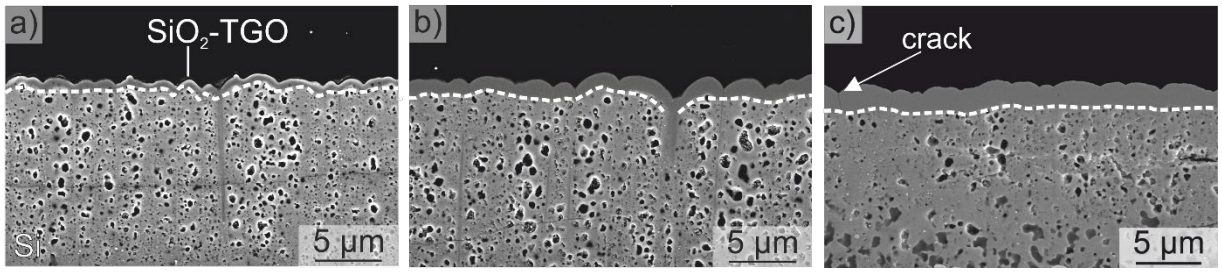

Fig. 4. Evolution of the TGO layer of coating system, deposited on Mo-9Si-8B alloy, in the form of SEM cross-sectional images; a) after 10; b) 100; c) 300 hours at 1200 °C.

Since Mo shows pest oxidation in the intermediate temperature zone, further testing was carried out at a temperature of 800 °C for 100 hours to proof the pesting resistance. A homogeneous and almost pore-free microstructure of the Si top layer was found after testing (Fig. 5 a)). The columnar structure of the Mo-Si

interlayer has been largely preserved. EDS measurements show up to approx. 40 at.% O in the interstitial spaces between the columns (Fig. 5 b)). The alloy remained almost unaffected by diffusion processes in the interface between layer and substrate, so that no visible formation of an interdiffusion zone can be observed. Furthermore, a local, discontinuous formation of a thin Si-oxide layer on the surfaces of the Si top layer. Element distribution images from EDS analysis show an increased oxygen concentration in these areas.

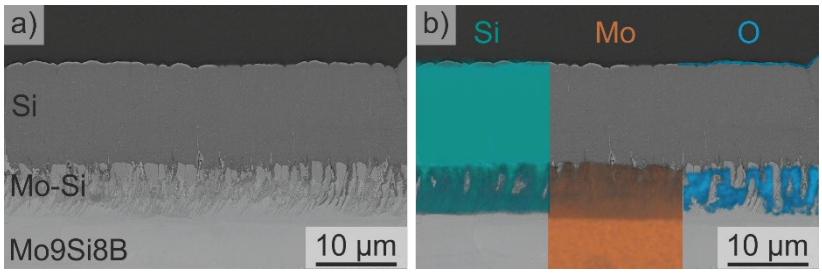

Fig. 5. SE detector SEM of the dual layer system's microstructure, deposited on Mo-9Si-8B, after 100 isothermal exposure time at 800 °C; a) cross-sectional images; b) EDS element mapping.

In addition to quantitative EDS analysis, X-ray diffraction helps to identify individual phases within the dual layer system. Fig. 6 shows the diffractograms of the dual layer system in the as-coated state, deposited on the Mo-9Si-8B substrates. After deposition, the Si top layers are partially X-ray amorphous. This is indicated by the slight formation of an amorphous hill in the XRD scan. However, the first smaller peaks of crystalline or semi-crystalline silicon can also be detected. Furthermore, the phases Mo_5Si_3 and $MoSi_2$ are present in the as-coated state, which can be traced back to the Mo-Si interlayer because neither TZM nor Mo-9Si-8B contain those phases. In this case, as well as in the following section of this work, α-$MoSi_2$ is the polymorph in which $MoSi_2$ occurs. Despite a total layer thickness of approx. 20 µm, a clear molybdenum peak can also be seen in the diffractogram. This peak can be assigned to the Mo_{ss} phase of the Mo-9Si-8B substrate. After the crystallization annealing process at 900 °C for 1 hour and subsequent oxidation experiments at 1200 °C for 10 hours, two distinct crystalline Si peaks can be seen in the diffractogram (Fig. 6) of the dual layer system. In parallel, SiO_2 can be detected starting at a holding time of 100 hours. This is the α-cristobalite. Also, in further investigations of this work, unless otherwise described, SiO_2 is α-Cristobalite. After 300 h of testing the Mo_{ss} peak increases drastically which could be related to the local failure, see in Fig. 10.

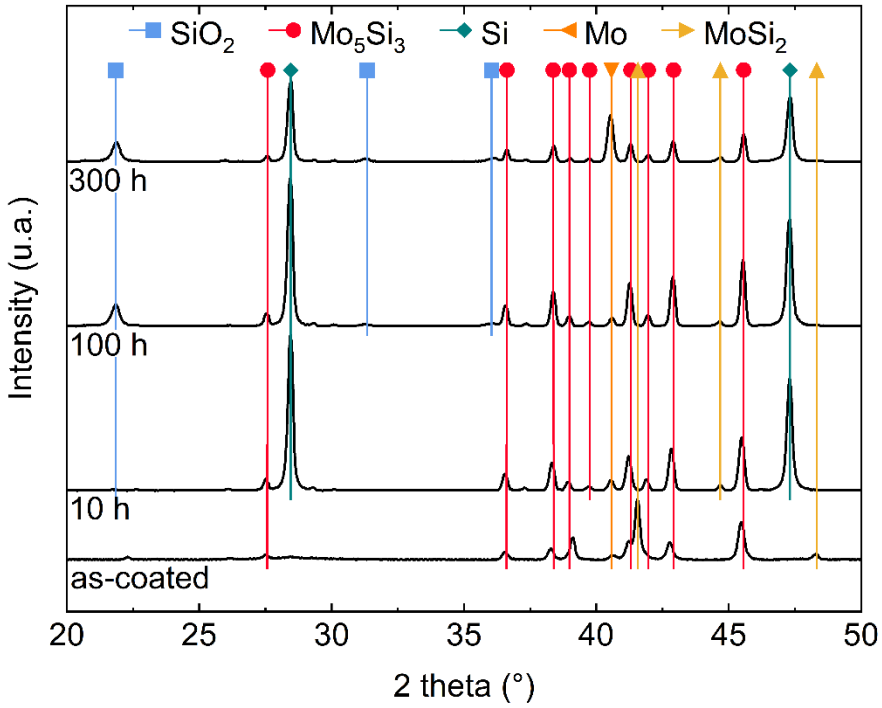

Fig. 6.XRD scans of the dual layer system, deposited on the Mo-9Si-8B, after deposition in the as-coated state, after 10, 100 and 300 hours of ageing at 1200 °C.

Fig. 7 shows the XRD scans of the layer system on the Mo-9Si-8B alloy, after the oxidation test at 800 °C for 100 hours in air with the crystallization heat treatment. The dominate peaks seen here is the Si due to the Si top layer. The Mo_5Si_3 and $MoSi_2$ peaks belong to the interlayer, the Mo peak belongs to the substrate material. The small SiO_2 peak indicates most likely, a local, discontinuous formation of a thin Si-oxide layer on the surface.

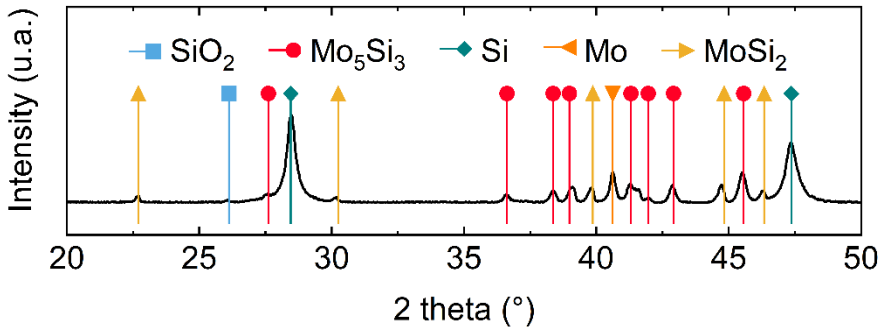

Fig. 7. XRD scan of the dual layer system, deposited on the substrate Mo-9Si-8B, after 100 hours aging at 800 °C.

In order to analysis the layer thickness development, image processing software has been used. In addition, the growth of the TGO layers was evaluated. Fig. 8 a) shows the determined layer thicknesses of the dual system in the as-coated state, deposited on the TZM substrate, as well as after 10, 100 and 300 hours of ageing at 1200 °C and ageing for 100 hours at 800 °C, applied to the substrate Mo-9Si-8B. The thickness of the interlayer was thereby measured from the surface of the substrate until the end of the columns which look finger-like after oxidation testing. The darker phase in between the Mo-Si fingers is hereby considered as interlayer phase. The total coating thickness in the as-coated state was about 18 µm. After 10 hours of testing the total thickness increased by 6 µm overall to 24 µm. Up to a holding time of 100 hours, the thickness of the layer system on the substrate initially increases by up to approx. 5 µm to 23 µm. In the

further testing of up to 300 hours, the total layer thickness develops in the opposite direction to its previous layer thickness, resulting in a layer of approx. 22 µm after this holding time. Compared to the as-coated condition, however, a maximum increase of approx. 4 µm is shown. Whilst the layer thickness of the top layer continues decrease with increasing holding time, the opposite is true for the interlayer layer thickness (Fig. 8 a)). A reduction of 3 µm can be seen for the top layer after 30 hours of holding time compared to the sample after 10 hours of holding time. The interlayer presents a slight reduction in the layer thickness after 10 hours but increases again to almost the same as-coated thickness after 300 hours. This reduction is in the range of fluctuation due to curved columns and irregular interface. In addition to the oxidation test at 1200 °C, Mo-9Si-8B samples were also exposed for 100 hours at 800 °C representing an increase of the complete dual layer system of approx. 1 µm compared to the as-coated state. The measurement results of the interlayer as well as those of the top layer also show only a slight divergence of the layer thickness. The exact development of the layer thickness curves as a function of the duration of the oxidation tests is shown in Fig. 8 a) and b) below.

For the TGO layer, a nearly parabolic course of the layer thickness curve can be examined, which is mainly due to the parabolic growth kinetics of silicon dioxide. The TGO layers on the Mo-9Si-8B alloy with a maximum thickness of 1.54 µm exhibit low TGO growth after 300 hours at 1200 °C (Fig. 8 b)).

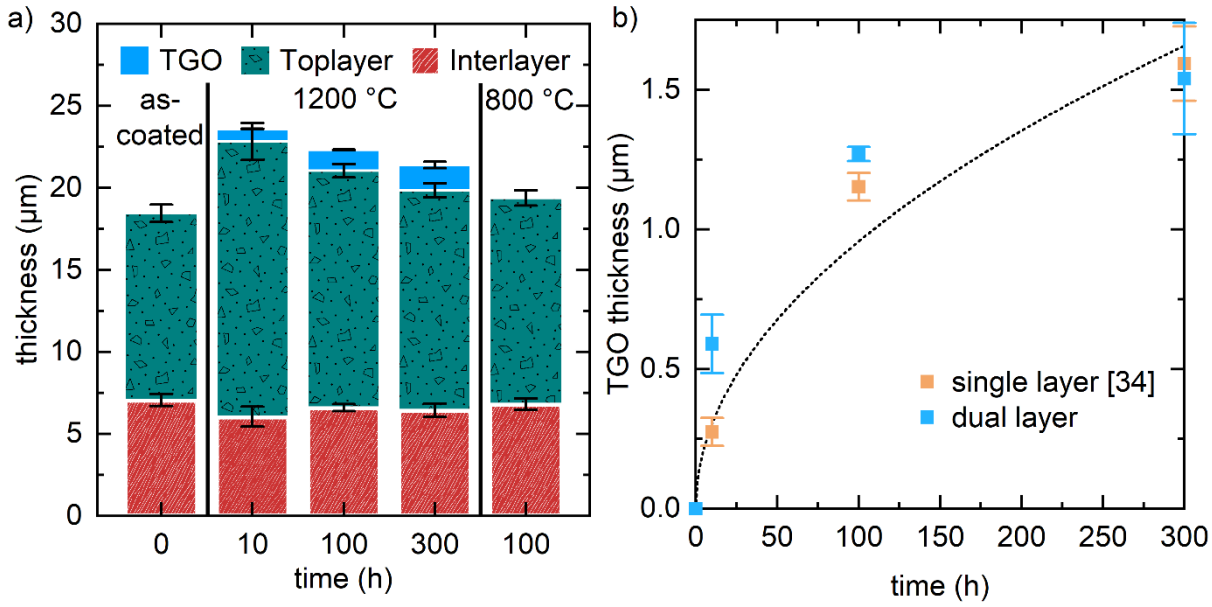

Fig. 8. Development of layer thickness over testing time; a) bar chart of the total layer system, the Si top layer, the graded Mo-Si interlayer and the SiO_2 TGO, deposited on the substrate Mo-9Si-8B, after the oxidation tests and in the as-coated state on TZM at 1200 °C and 800° C; b) TGO thickness over testing time at 1200 °C with a parabolic trendline.

Due to the weight measurements after the respective holding times of 10, 100 and 300 hours, it is possible to determine the change in mass in relation to the sample surface compared to the initial state. Fig. 9 shows the weight curves of both uncoated and coated substrate alloy after the isothermal oxidation tests at 1200 °C and at 800 °C. In order to explain the mass losses more clearly, macro images of the coated samples are provided in Fig. 10. For every time frame, a new specimen has been used. Due to a manufacturing failure, the sample after 300 h is slightly smaller in dimension, shown in Fig. 10.

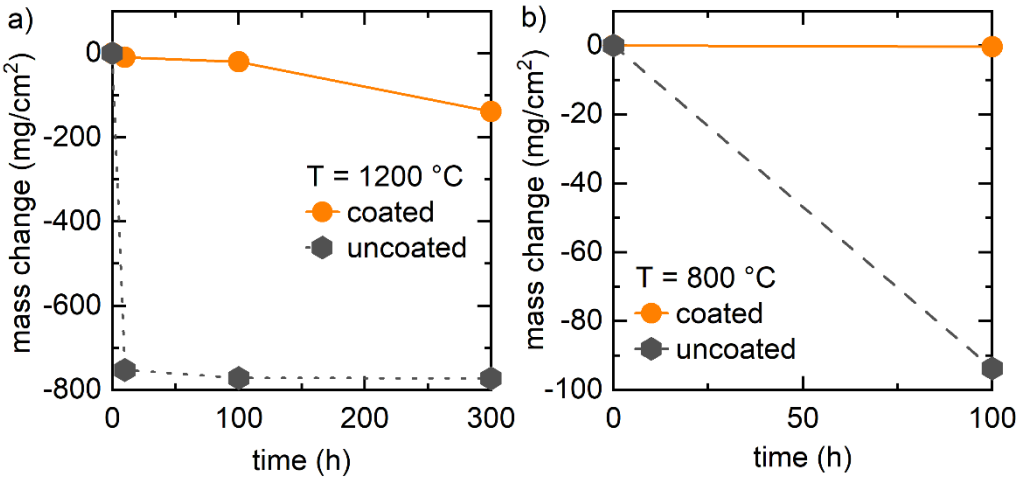

Fig. 9. Mass change versus time of uncoated and coated Mo-9Si-8B sample related to the sample surface after oxidation tests; a) at 1200 °C; b) at 800 °C in air.

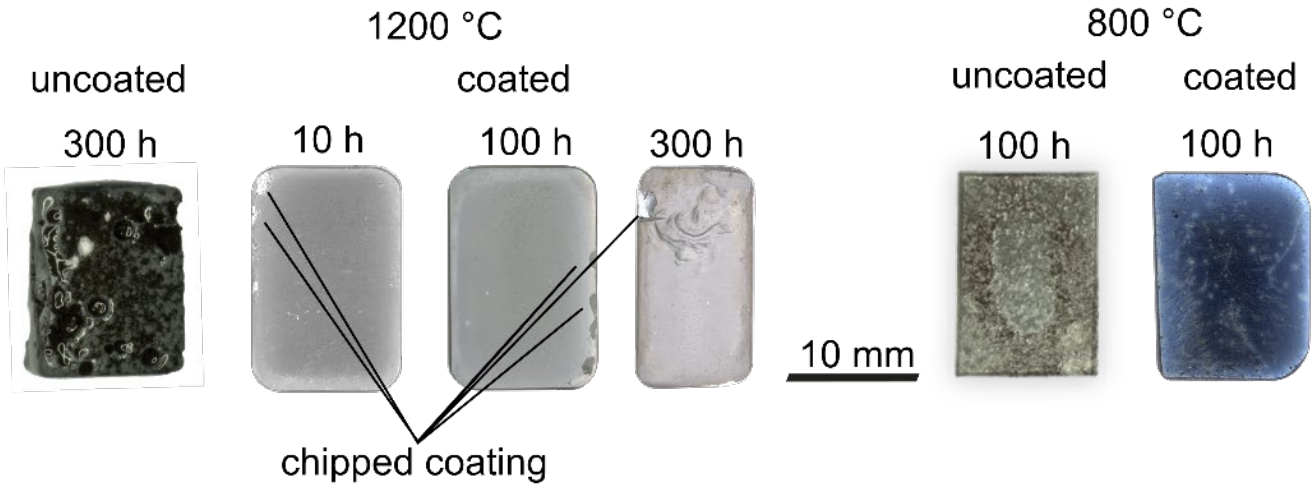

Fig. 10. Makro images of the isothermal tested uncoated and coated Mo-9Si-8B alloy.

After 10 hours holding time at 1200 °C, the uncoated Mo-9Si-8B shows the highest loss of mass overall with approx. 62 %. In the further course of time an almost stable behaviour with a further weight loss of around 3 % has been measured. Fig. 10 shows the uncoated Mo.9Si-8B substrate which turned black after the oxidation. The weight curve of the coated Mo-9Si-8B alloy reveals a progressive falling behaviour with increasing holding time. This results in a weight loss of approx. 21 % after the oxidation test for 300 hours at 1200 °C. The mass change related to the sample surface is reduced from - 773 to - 138 mg/cm^2 for the coated Mo-Si-B alloy in comparison to the uncoated substrate. This results in an improvement of the mass reduction of approx. 82 % for the coated alloy. The weight loss of the coated samples can be related to Fig. 10. After 10 h and 100 h, slight chipping/spallation of the coating at the edges is visible. After 300 h, the coating starts wrinkling and a hole is visible at the left upper edge. The weight loss of the coated sample after 100 hours holding time at 800 °C are only marginal with a maximal decrease of 0.05 % for the substrate. The macroscopic images of this sample shown in Fig. 10 reveals a blue colour and no visible failure or chipping of the coating. In contrast, the uncoated sample shows a catastrophic mass reduction with approx. 65 % weight loss at 800°C, see Fig. 9 b). In contrast to the massive weight loss the sample still stays in form but its surface shows the impact of the oxidation test.

3.3. Interdiffusion zone and phase analyses

In addition to the diffusion processes within the layer or in between interlayer and top layer, an interdiffusion zone (IDZ) is also formed within the Mo-9Si-8B substrate material close to the interface to the coating. This IDZ grows with increasing aging time towards the substrate interior. Fig. 11 shows the interface area layer-substrate for the holding times of 10, 100 and 300 hours. The IDZ is colored red for better visual perception. The thickness of this zone ranges from approx. 3.3 µm for a holding time of 10 hours (Fig. 11 a)) to a thickness of 7.2 µm for a holding time of 300 hours (Fig. 11 c)). By means of EDS measurements, approx. 70 at.% Mo and 30 at.% Si could be detected in the IDZ. Furthermore, it has been proven with EDS measurements that SiO_2 forms around the Mo-Si columns and later on the Mo-Si islands, shown in dark grey in the close-up images highlighted by the blue lines (Fig. 11 b) and c)). At the original interface between layer and substrate, SiO_2 precipitates in round shapes can also be detected.

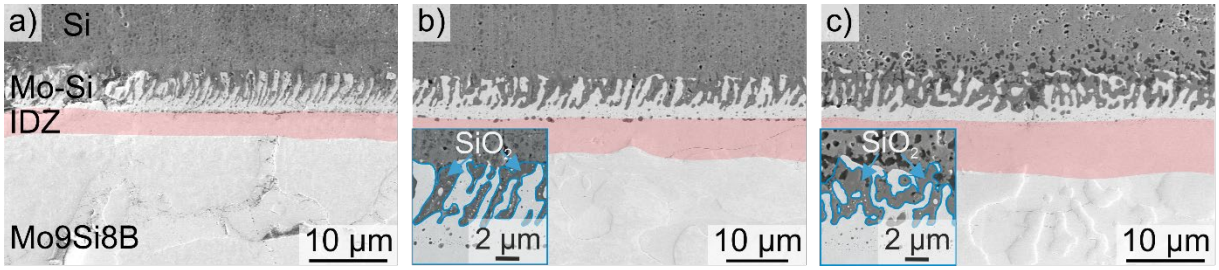

Fig. 11. SE dectector SEM cross-sectional images showing the dual layer system evolution of the interdiffusion zone, deposited on the Mo-9Si-8B, after a) 10, b) 100 and c) 300 hours of isothermal exposure to 1200 °C in air. In addition close up images of the interlayer-top layer area are presented after 100 and 300 h respectively.

Fig. 12 shows EDS line scans starting at the substrate material and ending in the Si top layer for the oxidation testing times of 10, 100 and 300 hours. The thickness of this zone is approx. 3.3 µm for a holding time of 10 hours (Fig. 12 a)) and increases to about 5 µm after 100 hours holding time (Fig. 12 b)) until ending after 300 hours at a thickness of about 10 µm (Fig. 12 c)). Starting from the substrate the Mo content gradually decreases until fading out in the Si top layer while the Si content increases. The gradation of the interlayer is still traceable, although the structure changes in time. At the original interface between IDZ and interlayer, round SiO_2 precipitates can be detected. Within the columnar gaps of the Mo-Si interlayer, SiO_2 is clearly measurable by EDS in all three line scans. The oxygen content decreases in the Si top layer but is still measurable due to pores within the top layer. In Fig. 12 a), an IDZ consisting of Mo and Si in a concentration that fits to the silicide Mo_3Si and Mo_5Si_3 is measurable. Fig. 12 b) shows an IDZ where the concentration of only Mo_3Si is measured. In Fig. 12 c) after 300 h the IDZ only contains the concentration that fits to the Mo_5Si_3 phase.

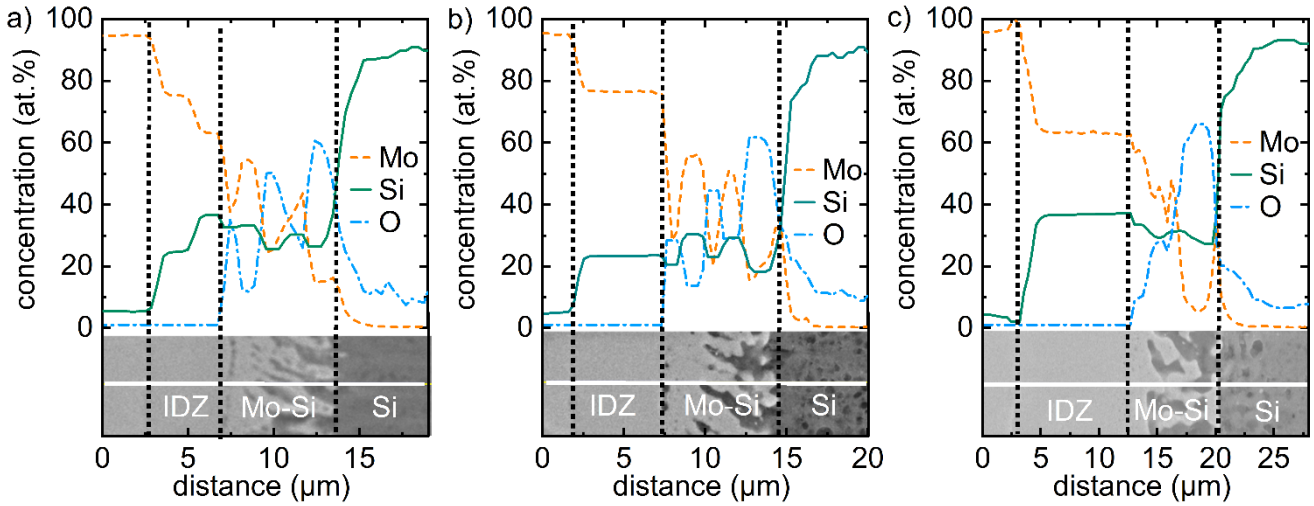

Fig. 12. SEM-EDS line scan in at.% showing the dual layer system evolution of the interdiffusion zone, deposited on the Mo-9Si-8B, after a) 10, b) 100 and c) 300 hours of isothermal exposure to 1200 °C in air.

For a precise phase analysis of the IDZ, detailed TEM analyses has been performed in the dual layer system on Mo-9Si-8B after 300 h at 1200 °C exposure in air. The region of interest for further in-depth analyses is marked in Fig. 13 a) which is situated in the transition between interlayer and IDZ, recognizable by the bright round inclusions. On the left side the SiO_2 from the interlayer coating is partly shown which evolved in between the Mo-Si columns (Fig. 13 a), b), d)). The Si from the interlayer is heavily oxidized, which matches with the SEM results given in Fig. 11. Moreover, the EDS mapping (Fig. 13 b), c), d)) shows no distinguished inhomogeneous parts in the Mo-Si interlayer and also in the IDZ. Therefore, Mo-silicide phases can be assumed. The oxygen mapping (Fig. 13 d)) indicates the bright inclusions as SiO_2 precipitates. In Fig. 13 e), f), g) and h) four grains have been identified using electron diffraction. The Mo-Si interlayer still contains the phases $MoSi_2$ (Fig. 13 e)) and Mo_5Si_3 (Fig. 13 f)) as-coated. $MoSi_2$ has been found closer to the SiO_2 phases and Mo_5Si_3 closer to the IDZ which indicates that the gradation of the interlayer still exists. The phase Mo_3Si was identified in locations at the former interface between interlayer and substrate (Fig. 13 g)). The grain consisting of the Mo_5Si_3 phase (Fig. 13 h)) is located in the IDZ of the Mo-9Si-8B substrate material, which is also no original phase of the Mo-9Si-8B alloy. Furthermore, the substrate material provides a coarser microstructure in comparison to the coating material.

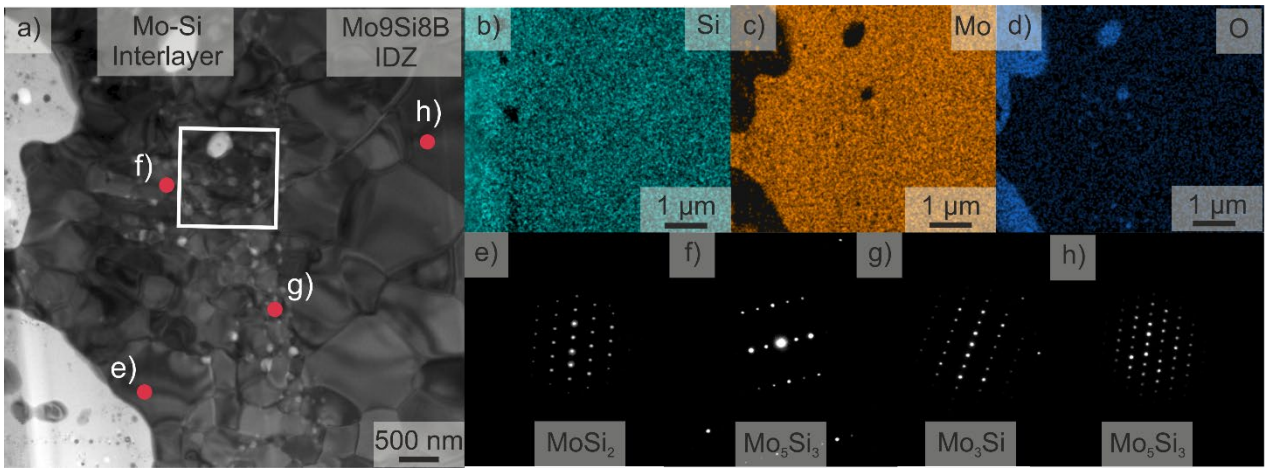

Fig. 13.TEM analyses of the coated Mo-9Si-8B alloy after 300 h of oxidation at 1200 °C; a) TEM bright field image of the Mo-9Si-8B IDZ and Mo-Si interlayer with marked ROI for further analysis; b) – d) EDS element mappings of the ROI showing the Si, Mo and O parts; e) – h) SAD pattern of the in a) marked grains.

The SiO_2 particles already identified in their chemical composition (Fig. 13 b) – d)) are analysed in terms of their allotropes in Fig. 13. In the diffractogram (Fig. 6) only crystallin SiO_2 in the form of cristobalite could be found. Fig. 14 a) shows the region of interest which includes a particle of SiO_2 of about 300 nm diameter in the IDZ clearly verified by the EDS mapping in Fig. 14 b) – d). This particle has the same thickness as the lamella itself. All the other SiO_2 particles are even smaller than the thickness of the lamella and seem to appear close to the interface between the IDZ and the Mo-9Si-8B substrate matrix. To identify the allotropes of the SiO_2 particles convergent beam electron diffraction (CBED) technique has been used. Since the particles are too small and the amount of the particles is too low, Debye-Scherrer technique could not be executed. Furthermore, it should be mentioned that the matrix is not oriented in zone axis to emphasize the haziness of the higher order Laue zone (HOLZ) line in the direct beam due to amorphous SiO_2 particle. Fig. 14 depicts the CBED patterns of the marked spots (1-4). Firstly, the CBED pattern (Fig. 14 e)) of the large SiO_2 particle (position 1) shows no evidence of elastic scattering of electrons by lattice. Only a halo is visible around the direct beam (bright centre spot), which indicates that the electrons are scattered randomly by an amorphous structure of material [37]. Therefore, it can be concluded that this is an amorphous SiO_2 particle, which has the same thickness as the sample itself. In contrast, at beam position 2 (a), the direct beam and the HOLZ lines of the matrix are clearly visible. When moving the beam onto an SiO_2 particle (position 3) but still positioned in the same grain, the HOLZ lines does not change but the HOLZ lines become more diffuse, which is indicative of amorphous (Fig. 14 g)). Lastly, the pattern at position 4 (Fig. 14 h)) displays just diffused HOLZ lines of the matrix, as two SiO_2 particles overlap at this position. The series of CBED patters (f-h) compared to pattern e), indicates that those are amorphous SiO_2 particles in the TEM lamella, since HOLZ lines becomes more diffuse as the particle occupies more of the sample cross section.

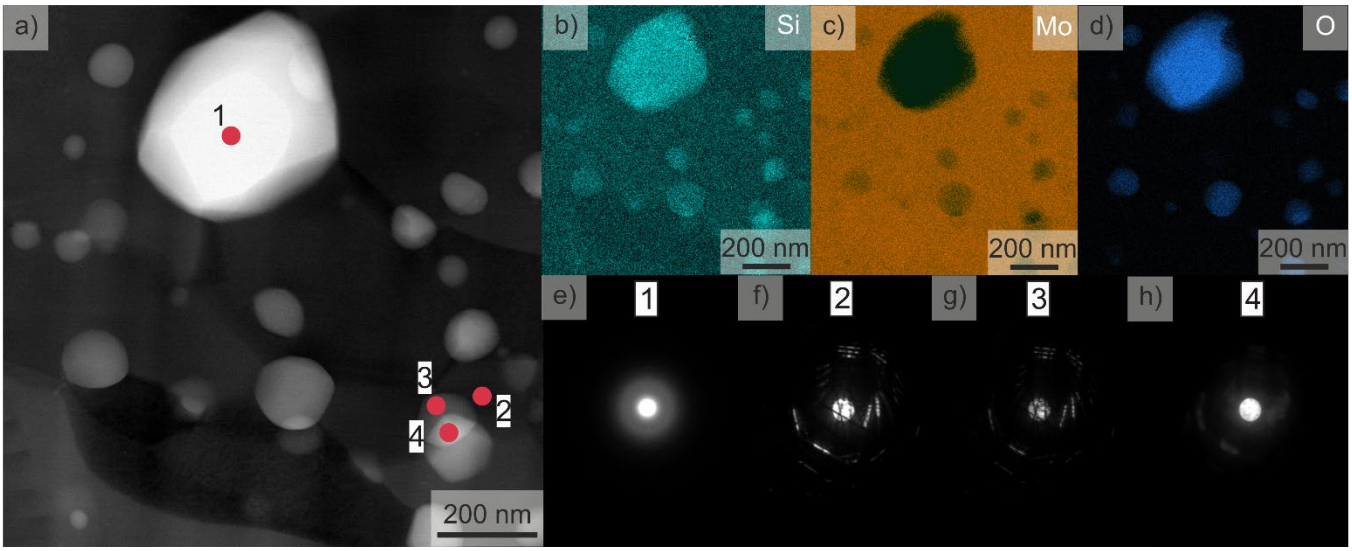

Fig. 14. TEM analyses of the Mo-9Si-8B lamella in the ROI from Fig. 13; a) STEM dark field image of the Mo-9Si-8B ROI with SiO_2 particles; b) – d) EDS mapping of the ROI showing the Si, Mo and O parts in at.%; e) – h) Nanobeam diffraction results; e) Ronchigram of amorphes SiO_2; f) Ronchigram of crystallin area Mo-9Si-8B;. g) Ronchigram of amorphes SiO_2 particles with crystallin Mo-9Si-8B; g) Ronchigram of two overlapping amorphes SiO_2 particles.

4. Discussion

4.1.Oxidation kinetics of the dual layer system

The coating system was able to reduce the mass loss of the Mo-9Si-8B alloy from 62 % to 21 % compared to the uncoated alloy after 300 hours of ageing at 1200°C. It must be noted that the evaluation of only three data points and the small spallation of the coating on edges, and the existence of a small un-coated area necessary for holding the samples may have affected the results.

After coating deposition, the samples were first subjected to a recrystallisation annealing process before the oxidation tests were carried out immediately afterwards. The main task of the Si top layer system was to protect the substrate materials from oxidation by forming a slow growing silica on top. For this reason, the formation of a silica TGO layer achieved in the current study under all conditions on the coating is quite promising, as a dense protective layer is realised between atmosphere and material. Cristobalite was the only SiO_2-allotrope that has been proven with XRD scans (Fig. 6) in this TGO layer after exposure at 1200° C. Although the temperatures shown in the phase diagram are higher for cristobalite formation under equilibrium conditions, the results here compare well with studies of similar Si coatings on monolithic SiC substrates deposited in a smaller laboratory coater [38-40].The potential reasons for favoured cristobalite formation at lower temperatures are discussed in greater detail by Opila [41]. Due to spalling of the coating system at the rims of the flat specimens, the determination of the mass change did not allow any conclusion to be drawn about an oxidation mechanism of the TGO layers. The observation of the TGO layer thicknesses, plotted over the holding time, however, showed a diffusion-controlled nearly parabolic growth rate (Fig. 8 b)). Investigations suggested that a correlation between the layer thickness and the mass change in relation to the surface can be determined [38, 42]. According to this, also oxygen inward diffusion-controlled oxidation can be assumed to be the dominant oxidation mechanism for the development of the SiO_2 TGO layers. In a previous study a Si-coating on a Mo-9Si-8B substrate without an interlayer was investigated [34]. Although the Si coatings were greater in thickness than the ones described here, the

growth of the TGO in thickness is in good agreement with the current results, see Fig. 8 b). There, the TGO thickness after 10 hours of testing at 1200 °C with the same parameters was slightly lower with about 0.25 µm compared to the 0.76 µm found here. This offset in data can be explained due to the formation of additional SiO_2 bubbles in the former study which were not taken into account for thickness determination in [34]. The implementing of an interlayer in this work fully prevented the formation of silica bubbles on top of the TGO that indicated a suppression outward diffusion of Mo-oxides. This was a great indicator for an improved oxidation protection due to the implementation of the Mo-Si graded interlayer in the coating system.

A critical TGO layer thickness for silicon layers on a SiC substrate produced by PVD, from which so-called mudcracks and local spallation due to crack propagation occurred, has been determined in a previous study. The critical TGO thickness was determined at a value of 4 – 5 µm. [38] The TGO layer of this work was with a maximum layer thickness of approx. 2 µm after 300 hours at 1200°C below this critical limit value and therefore showed no layer spalling and delamination. However, segmentation cracks in the TGO layers were occasionally visible after 300 hours of holding time at 1200 °C. These cracks can be attributed to thermally induced biaxial stresses due to the diverging coefficients of thermal expansion of silicon (2.6 10^{-6} 1/K, 25 °C) and the polymorphism of SiO_2. Cristobalite thus transformed from the β phase (3.1 10^{-6} 1/K) to the α phase (10.3 10^{-6} 1/K) during the cooling process at approx. 220 °C. This was accompanied by a specific volume reduction of 2.8 - 4.5 % [39, 43]. The decreasing layer thickness of the Si top layer was primarily due to the formation of the TGO layer since the SiO_2 grows mostly inwardly into the Si top layer. The diverging coefficients of thermal expansion of silicon and SiO_2 as well as the conversion from β- to α-cristobalite and the associated change in the coefficient of thermal expansion lead to significant stresses within the layer system. Overall, Fig. 10 shows clearly that this was not a major issue except on the edges of the samples where coating spallation can occur. However, as shown in the weight measurements in Fig. 9, layer spalling did not only correlate directly with weight loss. In addition to the spalling, the formation of the TGO layer, the oxidation of the substrate material and the internal oxidation and the resulting oxidation products also contributed to the observed mass change. Consequently, it was difficult to trace the mass changes back to a specific mechanism. After 300 h the decrease in mass can be clearly attributed to the wire application point which had to be applicated for applying the coating on the samples all around. Fig. 10 clearly showed a hole at the upper left side where substrate oxidation had been started. The oxidation of Mo-9Si-8B was accompanied by a large volume reduction in addition to the mass reduction. This could lead to the formation of compressive stresses within the layer, which opposed the volume reduction of the substrate. It can therefore be assumed that the compressive stresses lead to a compression of the coating material and finally to wrinkling when a critical stress was exceeded after 300 h at 1200°C in Fig. 10. Beneath the wrinkles, the coating was intact and no chipping could be detected which shows the layer system provides an excellent protection. Still, a reduction of 82 % in mass decrease was also achieved for the samples of the Mo9-Si-8B alloy compared to the uncoated substrate (Fig. 9). The results clearly indicated that a full coverage of Mo-based alloys by a coating is mandatory as well as improved oxidation behavior of the alloy itself which can be achieved by proper adjustment of the alloy composition [22, 35, 44].

Pesting in the temperature range of 800 °C could also be completely suppressed for the maximal tested time of 100 hours at 800 °C. Moreover, a dense Si layer with only slight porosity in the interlayer area was achieved. Despite an oxygen content of up to 45 at.% within the interlayer, no oxide phases were detected (Fig. 5). However, the XRD measurements indicate the presence of SiO_2 phases (Fig. 7) which could also

relate to a formation of SiO_2 at the surface of the Si top layer. This suggested that only minor diffusion processes have taken place during the ageing process. The layers did not show cracks. Furthermore, mass changes of only about 0.05 % was determined in Fig. 9. Fig. 10 provided proof by showing an unharmed blue reflecting coated sample. Therefore, the coating system provided excellent protection against oxidation for the alloy at temperatures around 800 °C. The coating suppressed successfully the pest oxidation that was a preferred occurrence in this temperature range.

4.2. Interface reactions between the Mo-9Si-8B alloy, the Mo-Si interlayer and Si top layer

By deposition a two-layer system not only the interface coating-substrate was of interest, but also the top layer-interlayer interface reaction. With increasing ageing time at 1200 °C a growing silicon rich IDZ was detected at the first interface. Between interlayer and top layer SiO_2 phases formed hindering oxygen to attack the substrate material. In the initial state, the EDS combined with XRD measurements indicate that the Mo_5Si_3 phase was present in the interlayer for most areas. The composition of the upper third of the interlayer suggests that it is mainly composed of the $MoSi_2$ phase until the pure Si coating follows (Fig. 2). Due to the gradation of the element molybdenum during the deposition as well as the high oxygen content within the interlayer, a clear phase assignment was not clearly possible. However, the XRD scan of the initial state confirmed the presence of the phases Mo_5Si_3, $MoSi_2$ in the layer system (Fig. 6). Therefore, it was obvious that the interlayer has been crystalline directly after magnetron sputtering using a substrate temperature of around 500°C (T_s). This is a great advantage since a change in volume accompanied by pore formation due to the transition from amorphous to crystallin was avoided. Since the Mo-Si interlayer was primarily composed of the phases Mo_5Si_3 and $MoSi_2$ and taking into account the respective melting points ($T_m(Mo_5Si_3)$ = 2180°C [45], $T_m(MoSi_2)$ = 2030°C [46]), the homologous temperature ($T_h=T_s/T_m$) was around 0.32. These values for T_h can be located in zone 2 of the structural zone model, which has a rough columnar structure. In this zone widening of columns and mis grown columns can also occur [47, 48]. Already in the initial state up to 20 at.% oxygen could be detected in the interlayer by EDS (Fig. 2). This proportion was probably implemented in the layer during the magnetron sputter process. So far, an oxygen contamination of the sputtering target could be excluded. Due to the high deposition temperature, oxygen contamination of the gas supply system or contamination from the heating system could be possible. Already after oxidation testing of 10 hours at 1200 °C the columnar gaps in the interlayers as well as in the silicon layer had closed due to internal oxidation, leading to the formation of internal SiO_2 (Fig. 12 a)). The formation of SiO_2 can be attributed to the stored oxygen content in the interlayer. With increasing oxidation time, the SiO_2 phase grew along the columnar structure of the interlayer and formed an almost continuous SiO_2 area between interlayer and top layer (Fig. 12 b), c)). Additionally, some oxygen could potentially be introduced into the coating system by migration along the vertical column boundaries before the Si top layer formed the dense TGO. Due to a significantly lower Gibbs energy of SiO_2 ($\Delta_fG°(SiO_2)$ = -853.67 kJ - mol^{-1} [49]) compared to the $MoSi_2$ ($\Delta_fG°(MoSi_2)$ = -146.3 kJ - mol^{-1} [50]) and the Mo_5Si_3 ($\Delta_fG°(Mo_5Si_3)$ = -312.9 kJ - mol^{-1} [50]) phase which are preferentially present in the Mo-Si phase diagram [51] at 1200 °C, SiO_2 was formed preferably. In later stages, SiO_2 then slowed down the oxygen diffusion towards the substrate because of its slow oxygen diffusion [38]. Rastogi et al. were able to demonstrate in their investigations that the formation of an SiO_2 layer at a silicon-molybdenum interface impedes the formation of Mo-silicides [42]. These results were consistent with the XRD scans in this work. With increasing holding time, a reduction of the $MoSi_2$ phase peaks could be detected (Fig. 6). Thus, a slow successive dissolution of this phase within the interlayer occurred. According to Tortorici et al., the $MoSi_2$ phase was formed preferentially during the heat treatments of Mo-Si diffusion pairs [52]. This effect was

not observed in this work, since the Si diffusion form the Si top layer in the direction to the interlayer was probably reduced by the formation of SiO_2. On the other hand, the comparatively high Mo and low Si concentration in the substrate alloys lead to silicon diffusion from the interlayer towards the Mo-9Si-8B substrate, which would explain the progressing dissolution of the Mo_5Si_3 and $MoSi_2$ phases in the interlayer. Sakidja et al. described in their investigations the complete dissolution of a 15 µm thick $MoSi_2$ layer produced by pack cementation on top of a Mo-14.2Si-9.6B substrate with the formation of a Mo_5Si_3 phase after 50 hours of ageing at 1200 °C [24]. Tang et al. made similar observation and postulated that the lifetime of the $MoSi_2$ coating is limited by the Si depletion due to diffusion into the substrate material [53]. This statement also agrees with the XRD data in this work (Fig. 6) and the EDS line scans in Fig. 12. Already after a holding time of 10 hours $MoSi_2$ could hardly be detected. The line scan in Fig. 12 a) indicated Mo_3Si and Mo_5Si_3 in the IDZ, in the interlayer itself the phases could not be distinguished easily due to the heterogenous phase formations of SiO_2 and Mo-silicides. Extended holding times showed in Fig. 12 b) an IDZ with the composition of Mo_3Si only. Since the Mo-9Si-8B alloy contains three phases, this IDZ line scan probably evolved in contact with the Mo_{ss} phase instead of a Mo_3Si or Mo_5SiB_2 phase. Due to the high difference in Si concentration between coating system and Mo_{ss}, the diffused Si was most likely only enough to form the Mo_3Si phase. The IDZ is rather heterogenous and contains both phases Mo_3Si and Mo_5Si_3. In Fig. 12 c) an IDZ only showing the composition close to the Mo_5Si_3 was detected. This was in great agreement with the TEM findings described in Fig. 13. The Mo_{ss} phase which is usually the main content with over 50 vol% in the Mo-9Si-8B substrate material could not be found in the IDZ. In contrast to our previous findings for a Si-coating without an intermediate layer, where a homogenous IDZ of about 5 – 8 µm after 300 h at 1200 °C consisting of Mo_3Si phase was found as described in [34], the present dual layer coating formed two Mo-silicide in the IDZ and changed the phase structure in the substrate up to a depth of 10 µm after 300 hrs of oxidation at 1200 °C. The TEM results are in great agreement with the line scans. The phases $MoSi_2$ and Mo_5Si_3 analysed in Fig. 13 e) – f) were formed through magnetron sputtering. They are a proof of the still existing gradation of the interlayer. Fig. 13 g) identified as Mo_3Si could be an original phase from the Mo9Si8B or was originally an Mo_5Si_3 phase of the interlayer and has been reduced to Mo_3Si due to the SiO_2 precipitates. Fig. 13 h) identified as Mo_5Si_3 cannot be found originally in the Mo9Si8B alloy and lies within the IDZ. This showed that the silicon interdiffusion is changing the Mo-phases at the surface of the substrate. Although the IDZ was greater in thickness than in the previous study of magnetron sputtered pure Si coating on Mo-alloys, the adhesion of the dual layer system in this work has been increased. In Fig. 11 a) – c) small round shaped precipitates were noticeable throughout the interface between interlayer and substrate. With increasing ageing time, they agglomerated to fewer and bigger particles. Fig. 14 a) showed that the precipitates are SiO_2. They are most likely formed with excess silicon in the interlayer and the stored oxygen there. The SiO_2 precipitates were mostly located at the grain boundaries and showed an amorphous crystal structure. Due to the lower Gibbs energy of SiO_2 compared to Mo-oxides it seems to be more likely that oxygen diffused along the grain boundaries and formed SiO_2 by reacting with the Si at the expense of formation of Si-rich Mo-silicide [54, 55].

The nano and micro porosity in the Si top layer can be attributed to the used substrate BIAS voltage and the resulting implementation of argon in the Si top layer during the sputtering process. Right after 10 h of isothermal testing the pores became visible (Fig. 3 a)). As a result of the evolving porosity, the Si top layer grows in thickness of up to 15 % compared to the its initial state (Fig. 8 a)). Right above the interlayer, increased pore formation occurred in the Si top layer after a holding time of 300 hours at 1200°C. Here, the diffusion of the silicon to the interlayer interface took place and the formation of SiO_2 began. Since silicon has a diffusion rate several orders of magnitude higher than that of molybdenum, the latter tried to diffuse

in the direction of the substrate despite the hindrance by the Si-oxide phase formed as a horizontal layer in the interlayer [56]. This well-known Kirkendall effect in which an imbalance of the diffusion coefficients or diffusivity occurred due to different atomic types of two elements leads to Kirkendall pores. They were also detected by Yoon et al. in $MoSi_2$/Mo diffusion pairs [57]. In the present investigation, those Kirkendall pores started to form after 300 hrs mainly in location right above the SiO_2 present in the interlayer

The grown IDZ supported the adhesion of the coating system and leads to a smooth transition between substrate and interlayer as already discussed. Within the Si top layer, the evenly distributed porosities induced by the BIAS voltage also helped to maintain the adhesion. The pores have been working to reduce thermal induced stress. This is necessary due to the CTE mismatch between Si (2.6 10^{-6} 1/K, 25 °C) and the substrate (5 – 6 10^{-6} 1/K) [58]. The durability of the coating could be especially seen in Fig. 10 after 300 h of testing at 1200 °C. Here not even the wrinkling of the coating lead to spallation showing that the coating was able to withhold great macroscopic changes. With increasing holding time, the pores agglomerated. This was in fairly good agreement with previous findings for sputtered Si layers in a smaller lab coater under 120 °C substrate temperature and 100 V BIAS [59].

5. Conclusions

In this study, a dual layer magnetron-sputtered coating system consisting of a graded Mo-Si interlayer and a Si top layer has been developed in order to provide sufficient oxidation protection of the Mo-based alloy Mo-9Si-8B at 1200°C for 300 hours. The interlayer has been constructed to create a thermodynamic equilibrium between alloy and Si top layer and therefore to enhance the adhesion. After deposition the interlayer at elevated temperature it was already crystalline while the Si top layer was amorphous. To decrease the thermal stresses created during testing between alloy and Si top layer, the top layer has been designed to form nanopores. The dual layer coating protected the Mo-9Si-8B alloy up until 300 h of isothermal exposition at 1200 °C in lab air by forming a dense thermally grown silica scale on top. The protective Si top layer showed excellent adhesion on the interlayer and substrate during prolonged oxidation. In the initial phase of oxidation, the SiO_2 formed as TGO on the top layer and at the interface between interlayer and top layer. The TGO had a nearly parabolic growth rate and increased with time in thickness.

Due to some oxygen that was incorporated in the interlayer during the PVD process silica formation progressed in this area during prolonged oxidation. Although this SiO_2 formed as a nearly dense horizontal layer at the interface between interlayer and top layer, the Si inward diffusion into the substrate could not be completely suppressed until 300 h. The coarse columnar microstructure of the interlayer after manufacture transformed gradually with the development of the SiO_2 phase. The Mo-Si gradation decreased gradually in thickness, thereby creating the interdiffusion zone. In the substrate, the created interdiffusion zone was silicon enriched and consisted of a variety of Mo-silicide. The pest oxidation usually occurring at intermediate temperatures of 800 °C was successfully inhibited by the dual layer coating system up to 100 h.

In comparison to a similar Si coating without interlayer, the formation of a dense TGO was faster and full covering in the beginning here and the overall performance could be improved. Grading the composition of the interlayer did not influence the behaviour of the Si top layer much but increased its stability towards the substrate by all means.

6. Prime novelty statement

We confirm that this manuscript has not been published previously by any of the authors and is not under consideration for publication in another journal.

7. Data availability statement

The raw and processed data required to reproduce these findings are available on request to ronja.anton@dlr.de.

8. Declaration of Competing Interest

The authors report no declarations of interest.

9. Acknowledgment

This work was conducted under the financial support of Deutsche Forschungsgemeinschaft (DFG) within the framework of grants no. SCHU 1372/7-2 and GO 2283/3-2 which is gratefully acknowledged. The authors are thankful for their project partners S. Obert, Dr.-Ing. A. Kauffmann and Prof. Dr.-Ing. M. Heilmaier for providing the substrate material and for scientific support. We thank Dr.-Ing. J. Müller from the University of Siegen for the TEM support. For the scientific and technical support at the German Aerospace Centre, the authors thank V. Leisner, P.-P. Bauer, J. Brien. For lamella preparation with FIB, we like to thank F. Kreps.

10. References

[1] J. H. Perepezko, The hotter the engine, the better, Science 326. 5956 (2009) 1068-9. 10.1126/science.1179327

[2] A. Lange and R. Braun, Magnetron-sputtered oxidation protection coatings for Mo–Si–B alloys, Corrosion Science 84. (2014) 74-84. 10.1016/j.corsci.2014.03.013

[3] M. R. Middlemas and J. K. Cochran, The microstructural engineering of Mo-Si-B alloys produced by reaction synthesis, JOM 62. 10 (2010) 20-24. 10.1007/s11837-010-0150-3

[4] J. H. Perepezko, High temperature environmental resistant Mo-Si-B based coatings, International Journal of Refractory Metals and Hard Materials 71. (2018) 246-254. 10.1016/j.ijrmhm.2017.11.033

[5] H. J. Grabke and G. H. Meier, Accelerated Oxidation, Internal Oxidation, Intergranular Oxidation, and Pesting of Intermetallic Compounds, Oxidation of Metals 44. 1-2 (1995) 147-176. 10.1007/Bf01046726

[6] J. H. Schneibel, C. T. Liu, D. S. Easton, and C. A. Carmichael, Microstructure and mechanical properties of Mo–Mo3Si–Mo5SiB2 silicides, Materials Science and Engineering: A 261. 1 (1999) 78-83. https://doi.org/10.1016/S0921-5093(98)01051-X

[7] J. Kruzic, J. Schneibel, R. J. M. Ritchie, and m. t. A, Ambient-to elevated-temperature fracture and fatigue properties of Mo-Si-B alloys: role of microstructure, 36. 9 (2005) 2393-2402.

[8] C. A. Sequeira, High temperature corrosion: fundamentals and engineering. John Wiley & Sons, 2019 978-0-470-11988-4.

[9] J. R. Nicholls, Designing oxidation-resistant coatings, Jom-Journal of the Minerals Metals & Materials Society 52. 1 (2000) 28-35. DOI 10.1007/s11837-000-0112-2

[10] J. J. Kruzic, J. H. Schneibel, and R. O. Ritchie, Fracture and fatigue resistance of Mo–Si–B alloys for ultrahigh-temperature structural applications, Scripta Materialia 50. 4 (2004) 459-464. https://doi.org/10.1016/j.scriptamat.2003.11.002

[11] J. H. Schneibel, C. T. Liu, L. Heatherly, and M. J. Kramer, Assessment of processing routes and strength of a 3-phase molybdenum boron silicide (Mo5Si3-Mo5SiB2-Mo3Si), Scripta Materialia 38. 7 (1998) 1169-1176. 10.1016/S0921-5093(98)01051-X
[12] D. A. Berztiss, R. R. Cerchiara, E. A. Gulbransen, F. S. Pettit, and G. H. Meier, Oxidation of Mosi2 and Comparison with Other Silicide Materials, Materials Science and Engineering a-Structural Materials Properties Microstructure and Processing 155. 1-2 (1992) 165-181. Doi 10.1016/0921-5093(92)90324-T
[13] I. Rosales, H. Martinez, D. Bahena, J. A. Ruiz, R. Guardian, and J. Colin, Oxidation performance of Mo3Si with Al additions, Corrosion Science 51. 3 (2009) 534-538. 10.1016/j.corsci.2008.12.004
[14] R. W. BARTLETT, J. W. McCAMONT, and P. R. GAGE, Structure and Chemistry of Oxide Films Thermally Grown on Molybdenum Silicides, 48. 11 (1965) 551-558. https://doi.org/10.1111/j.1151-2916.1965.tb14671.x
[15] K. Natesan and S. C. Deevi, Oxidation behavior of molybdenum silicides and their composites, Intermetallics 8. 9-11 (2000) 1147-1158. Doi 10.1016/S0966-9795(00)00060-1
[16] M. A. Azim, D. Schliephake, C. Hochmuth, B. Gorr, H. J. Christ, U. Glatzel, and M. Heilmaier, Creep Resistance and Oxidation Behavior of Novel Mo-Si-B-Ti Alloys, Jom 67. 11 (2015) 2621-2628. 10.1007/s11837-015-1560-z
[17] M. A. Azim, B. Gorr, H. J. Christ, O. Lenchuk, K. Albe, D. Schliephake, and M. Heilmaier, Effect of Ti content and nitrogen on the high-temperature oxidation behavior of (Mo,Ti) 5 Si 3, Intermetallics 90. (2017) 103-112. 10.1016/j.intermet.2017.05.023
[18] D. Schliephake, A. Kauffmann, X. Cong, C. Gombola, M. Azim, B. Gorr, H.-J. Christ, and M. Heilmaier, Constitution, oxidation and creep of eutectic and eutectoid Mo-Si-Ti alloys, Intermetallics 104. (2019) 133-142. 10.1016/j.intermet.2018.10.028
[19] S. Burk, B. Gorr, H.-J. Christ, D. Schliephake, M. Heilmaier, C. Hochmuth, and U. Glatzel, High-temperature oxidation behaviour of a single-phase (Mo,Ti)5Si3 (Mo–Si–Ti) alloy, Scripta Materialia 66. 5 (2012) 223-226. 10.1016/j.scriptamat.2011.10.042
[20] D. Schliephake, C. Gombola, A. Kauffmann, M. Heilmaier, and J. H. Perepezko, Enhanced Oxidation Resistance of Mo–Si–B–Ti Alloys by Pack Cementation, Oxidation of Metals 88. 3-4 (2017) 267-277. 10.1007/s11085-017-9730-8
[21] S. Obert, A. Kauffmann, S. Seils, S. Schellert, M. Weber, B. Gorr, H.-J. Christ, and M. Heilmaier, On the chemical and microstructural requirements for the pesting-resistance of Mo–Si–Ti alloys, Journal of Materials Research and Technology 9. 4 (2020) 8556-8567. https://doi.org/10.1016/j.jmrt.2020.06.002
[22] M. Weber, B. Gorr, H.-J. Christ, S. Obert, A. Kauffmann, and M. Heilmaier, Effect of Water Vapor on the Oxidation Behavior of the Eutectic High-Temperature Alloy Mo-20Si-52.8Ti, 22. 7 (2020) 2000219. https://doi.org/10.1002/adem.202000219
[23] J. H. Perepezko, T. A. Sossaman, and M. Taylor, Environmentally Resistant Mo-Si-B-Based Coatings, Journal of Thermal Spray Technology 26. 5 (2017) 929-940. 10.1007/s11666-017-0565-2
[24] R. Sakidja, J. Park, J. Hamann, and J. Perepezko, Synthesis of oxidation resistant silicide coatings on Mo–Si–B alloys, Scripta materialia 53. 6 (2005) 723-728.
[25] S. Majumdar, Isothermal and cyclic oxidation resistance of pack siliconized Mo–Si–B alloy, Applied Surface Science 414. (2017) 18-24. https://doi.org/10.1016/j.apsusc.2017.03.300
[26] S. Majumdar, I. Sharma, I. Samajdar, and P. Bhargava, Relationship Between Pack Chemistry and Growth of Silicide Coatings on Mo–TZM Alloy, Journal of The Electrochemical Society 155. 12 (2008) D734. 10.1149/1.2987954
[27] K. Choi, W. Yang, K.-H. Baik, Y. Kim, S. Lee, and J. S. Park, Growth Kinetics and Isothermal Oxidation Behavior of Aluminide Pack Coatings on a Multiphase Mo–Si–B Alloy, Oxidation of Metals 92. 5-6 (2019) 423-437. 10.1007/s11085-019-09930-0

[28] X. K. Deng, G. J. Zhang, T. Wang, S. Ren, Z. B. Li, P. Song, and Y. Shi, Characterization and oxidation resistance of B-modified Mo3Si coating on Mo substrate, Journal of Alloys and Compounds 807. (2019) 151693. ARTN 151693

10.1016/j.jallcom.2019.151693
[29] N. Nomura, T. Suzuki, K. Yoshimi, and S. Hanada, Microstructure and oxidation resistance of a plasma sprayed Mo–Si–B multiphase alloy coating, Intermetallics 11. 7 (2003) 735-742. https://doi.org/10.1016/S0966-9795(03)00069-4
[30] I. Smokovych, V. Bolbut, M. Kruger, and M. Scheffler, Tailored Oxidation Barrier Coatings for Mo-Hf-B and Mo-Zr-B Alloys, Materials (Basel) 12. 14 (2019). 10.3390/ma12142215
[31] I. Smokovych, G. Hasemann, M. Krüger, and M. Scheffler, Polymer derived oxidation barrier coatings for Mo-Si-B alloys, Journal of the European Ceramic Society 37. 15 (2017) 4559-4565. 10.1016/j.jeurceramsoc.2017.06.048
[32] A. Lange, R. Braun, and M. Heilmaier, Oxidation behavior of magnetron sputtered double layer coatings containing molybdenum, silicon and boron, Intermetallics 48. (2014) 19-27. 10.1016/j.intermet.2013.09.007
[33] A. Lange, R. Braun, and U. Schulz, PVD thermal barrier coating systems for Mo–Si–B alloys, Materials at High Temperatures 35. 1-3 (2017) 195-203. 10.1080/09603409.2017.1404686
[34] R. Anton, N. Laska, U. Schulz, S. Obert, and M. Heilmaier, Magnetron Sputtered Silicon Coatings as Oxidation Protection for Mo-Based Alloys, Advanced Engineering Materials 22. 7 (2020) 2000218. 10.1002/adem.202000218
[35] S. Obert, A. Kauffmann, and M. Heilmaier, Characterisation of the oxidation and creep behaviour of novel Mo-Si-Ti alloys, Acta Materialia 184. (2020) 132-142. 10.1016/j.actamat.2019.11.045
[36] M. Krüger, S. Franz, H. Saage, M. Heilmaier, J. H. Schneibel, P. Jéhanno, M. Böning, and H. Kestler, Mechanically alloyed Mo–Si–B alloys with a continuous α-Mo matrix and improved mechanical properties, Intermetallics 16. 7 (2008) 933-941. https://doi.org/10.1016/j.intermet.2008.04.015
[37] M. A. Asadabad and M. J. Eskandari, "Electron diffraction," Modern electron microscopy in physical and life sciences: IntechOpen, 2016. [Online].Available: https://www.intechopen.com/chapters/49537.
[38] R. Anton, V. Leisner, P. Watermeyer, M. Engstler, and U. Schulz, Hafnia-doped silicon bond coats manufactured by PVD for SiC/SiC CMCs, Acta Materialia 183. (2020) 471-483. 10.1016/j.actamat.2019.10.050
[39] B. T. Richards, S. Sehr, F. de Franqueville, M. R. Begley, and H. N. G. Wadley, Fracture mechanisms of ytterbium monosilicate environmental barrier coatings during cyclic thermal exposure, Acta Materialia 103. (2016) 448-460. 10.1016/j.actamat.2015.10.019
[40] V. Leisner, A. Lange, P. Mechnich, and U. Schulz, "MAGNETRON SPUTTERED Y2SiO5 ENVIRONMENTAL BARRIER COATINGS FOR SIC/SIC CMCS," presented at the HTCMC-9 & GFMAT 2016 Toronto, Ontario Canada, 2018.
[41] E. J. Opila, Oxidation Kinetics of Chemically Vapor-Deposited Silicon Carbide in Wet Oxygen, Journal of the American Ceramic Society 77. 3 (1994) 730-736. 10.1111/j.1151-2916.1994.tb05357.x
[42] R. S. Rastogi, V. D. Vankar, and K. L. Chopra, The Effect of Oxygen Impurity on Growth of Molybdenum Disilicide and Its Distribution during Rapid Thermal Annealing of Co-Sputtered Mosix Thin-Films, Thin Solid Films 213. 1 (1992) 45-54. Doi 10.1016/0040-6090(92)90473-O
[43] J. Rodríguez-Viejo, F. Sibieude, M. Clavaguera-Mora, and C. J. A. p. l. Monty, 18O diffusion through amorphous SiO2 and cristobalite, 63. 14 (1993) 1906-1908.
[44] S. Obert, A. Kauffmann, S. Seils, T. Boll, S. Kauffmann-Weiss, H. Chen, R. Anton, and M. Heilmaier, Microstructural and chemical constitution of the oxide scale formed on a pesting-resistant Mo-Si-Ti alloy, Corrosion Science 178. (2021) 109081. https://doi.org/10.1016/j.corsci.2020.109081

[45] M. Akinc, M. K. Meyer, M. J. Kramer, A. J. Thom, J. J. Huebsch, and B. Cook, Boron-doped molybdenum silicides for structural applications, Materials Science and Engineering: A 261. 1 (1999) 16-23. https://doi.org/10.1016/S0921-5093(98)01045-4
[46] Z. Yao, J. Stiglich, and T. S. Sudarshan, Molybdenum silicide based materials and their properties, Journal of Materials Engineering and Performance 8. 3 (1999) 291-304. 10.1361/105994999770346837
[47] J. A. Thornton, High-Rate Thick-Film Growth, Annual Review of Materials Science 7. (1977) 239-260. 10.1146/annurev.ms.07.080177.001323
[48] J. A. Thornton, Influence of apparatus geometry and deposition conditions on the structure and topography of thick sputtered coatings, Journal of Vacuum Science Technology

11. 4 (1974) 666-670.
[49] A. Heintz, "Thermodynamik der Mischungen und Mischphasengleichgewichte," in Thermodynamik der Mischungen: Mischphasen, Grenzflächen, Reaktionen, Elektrochemie, äußere KraftfelderBerlin, Heidelberg Springer Berlin Heidelberg, 2017, pp. 1-195. 10.1007/978-3-662-49924-5_1 978-3-662-49924-5.
[50] H. Fujiwara and Y. Ueda, Thermodynamic properties of molybdenum silicides by molten electrolyte EMF measurements, Journal of Alloys and Compounds 441. 1-2 (2007) 168-173. 10.1016/j.jallcom.2006.07.128
[51] H. Okamoto, Mo-Si (Molybdenum-Silicon), Journal of Phase Equilibria and Diffusion 32. 2 (2011) 176-176. 10.1007/s11669-010-9843-0
[52] P. C. Tortorici and M. A. Dayananda, Diffusion structures in Mo vs. Si solid-solid diffusion couples, Scripta Materialia 38. 12 (1998) 1863-1869. Doi 10.1016/S1359-6462(98)00111-0
[53] Z. Tang, A. J. Thom, M. J. Kramer, and M. Akinc, Characterization and oxidation behavior of silicide coating on multiphase Mo–Si–B alloy, Intermetallics 16. 9 (2008) 1125-1133. https://doi.org/10.1016/j.intermet.2008.06.014
[54] I. Barin, "Mg-Mo5Si3," in Thermochemical Data of Pure Substances Weinheim; New York: VCH, 1995, 1995, pp. 993-1079. https://doi.org/10.1002/9783527619825.ch12l
[55] I. Barin, "Si-SrWO4," in Thermochemical Data of Pure Substances Weinheim; New York: VCH, 1995, 1995, pp. 1480-1586. 10.1002/9783527619825.ch12q
[56] A. Paul, "Diffusion Rates of Components in Metal-Silicides Depending on Atomic Number of Refractory Metal Component," in Diffusion Foundations, 2019, vol. 21, pp. 29-84: Trans Tech Publ.
[57] J.-K. Yoon, G.-H. Kim, J.-Y. Byun, J.-S. Kim, and C.-S. Choi, Simultaneous growth mechanism of intermediate silicides in MoSi2/Mo system, Surface and Coatings Technology 148. 2 (2001) 129-135. https://doi.org/10.1016/S0257-8972(01)01354-8
[58] A. Lange, M. Heilmaier, T. A. Sossamann, and J. H. Perepezko, Oxidation behavior of pack-cemented Si–B oxidation protection coatings for Mo–Si–B alloys at 1300°C, Surface and Coatings Technology 266. (2015) 57-63. https://doi.org/10.1016/j.surfcoat.2015.02.015
[59] V. Leisner, "Neue Environmental Barrier Coatings für SiC/SiC-Faserverbundwerkstoffe durch PVD-Technologien," Ph.D. thesis, Karlsruher Institut für Technologie (KIT), 2020.